

Comprehensive test system for ship-model resistance and propulsion performance in actual seas

Jian-feng Lin, Da-gang Zhao ^{*}, Chun-yu Guo ^{**}, Yu-min Su, Xiang-hai Zhong

College of Shipbuilding Engineering, Harbin Engineering University, Harbin, 150001, China

ARTICLE INFO

Keywords:

Ship-model testing
Actual seas
Resistance and propulsion performance
Comprehensive test system
Energy-saving device

ABSTRACT

In this study, we developed a comprehensive test system for ship-model testing in actual wind, wave, and current flow environments. The resistance and propulsion performance of a 25-m-long ship model were analysed, and corresponding correction methods were developed to determine the performance in actual sea conditions. The effects of an energy-saving device on the ship performance under actual sea conditions were assessed using this platform. The proposed methodology and technique are reliable and promising, and can provide a basis for the development of new ship testing techniques.

1. Introduction

The water bodies that ships operate in are complex environments, making it difficult to accurately evaluate their comprehensive performance. The analysis of ship performance, development of new ship types, and design of high-performance ships have been considerably assisted by theoretical studies (Noblesse et al., 2013; Ribeiro and Guedes, 2013), numerical simulation calculations (Wang et al., 2018; Zhao et al., 2017), physical model testing (Bouscasse et al., 2013; Gong et al., 2019), actual ship testing (Andersen and Jensen, 2014; Nielsen and Strelidinsky, 2012), and other methods. However, all these research methods have their own defects, such as scale effects and high cost, which inevitably affect their results.

Many scholars have attempted to perform ship-model tests in real environments to obtain accurate data on ship performance. Grigopoulos and Katsaounis (2004) conducted experiments on the hydrodynamic characteristics of ship models in sheltered sea areas, focusing on ship seakeeping performance. Loukakis et al. (2005) reported ship-model testing at sea at the 24th International Towing Tank Conference (ITTC). Quintana (2007) considered the DDG-1000, a Zumwalt-class destroyer of the US Navy, and conducted several ship-model testing experiments in actual seas, focusing on the effects of human factors on the success of sea wars. Coraddu (2013) implemented ship-model testing with a 7.2-m-long naval vessel model in still lake

waters. They explored the asymmetric propeller behaviour of the twin-screw ship during navigation. Fossati et al. (2015) conducted experiments on ship motion and wave load in actual seas, using a 9.99-m-long yacht model. Sun et al. (2015) experimentally studied the seakeeping performance of two large-scale ship models with lengths of approximately 7 m. Jiao et al. (2018) comprehensively studied the seakeeping performance of a 12.5-m-long segmented ship model. However, the ship models used by these researchers had a maximum length of about 13 m; hence, there were still apparent scale effects. Moreover, to the best of our knowledge, no scholars have ever performed ship-model resistance tests in real sea environments; the previous self-propelled ship-model tests were typically carried out in sheltered sea areas or lakes, which lack realistic wind, wave, and current conditions.

In view of the above, we developed a new comprehensive testing system to assess the resistance and propulsion performance of ship models in actual seas. It can be used to study and analyse the performance of new types of ship, including high-performance ones. Combining the advantages of tank model testing and full-scale ship testing in actual seas, this new technique has considerable advantages:

- Testing occurs in an offshore environment with natural wind, wave, and current flow conditions, which means that the ship model can achieve the same sailing performance as in actual sea conditions. The

Abbreviations: ESD, energy-saving device; ITTC, International Towing Tank Conference; PSS, preswirl stator; GPS, global positioning system; INS, inertial navigation system; MoM, mean of means; DOF, degrees of freedom.

* Corresponding author.

** Corresponding author.

E-mail addresses: zhaodagang@hrbeu.edu.cn (D.-g. Zhao), guochunyu_heu@outlook.com (C.-y. Guo).

<https://doi.org/10.1016/j.oceaneng.2019.106915>

Received 29 March 2019; Received in revised form 1 December 2019; Accepted 31 December 2019

Available online 7 January 2020

0029-8018/© 2020 Elsevier Ltd. All rights reserved.

- six degrees-of-freedom (DOF) motions of the ship model are unconstrained during navigation, and the motion response characteristics are more realistic than those in tank testing.
- Effects such as refraction, diffraction, and breaking of waves in the ocean, and the related effects caused by wind and current flow can be considered. Tanks cannot simulate a real marine environment owing to the scale effects of wind, wave, and current flow and limitations of the wave-making capacity; waves in a tank have viscosities and surface tensions that are many times larger than real waves in the ocean, and artificial waves are affected by friction and reflection at the tank wall. In addition, the content of entrapped air bubbles in the free surface is relatively low. Wind scaling is also of significance, and the Reynolds number is not correctly simulated at the model scale, which means that inertial wind forces in the tank are proportionally smaller.
 - Unrestrained by the scale and functions of tanks, the ship model is largely free from model scale effects and the blockage effects of tanks.
 - A wide range of experiments can be implemented, including resistance and propulsion performance, seakeeping performance, manoeuvrability, and underwater explosion tests, in addition to experiments under complicated and dangerous working conditions.
 - More scientific, accurate, and reliable technical support can be provided for both the optimal design of the ship performance and the evaluation of comprehensive performance and application characteristics of platforms.

This comprehensive test system for the resistance and propulsion performance of a ship model in actual seas provides a new direction for the study of ship performance. To validate the developed testing technique, we conducted a series of tests on a 25-m-long ship model in actual seas in Qingdao, China (35.9°N , 120.2°E). The experiments included resistance, self-propulsion, partial seakeeping performance, and manoeuvrability tests. We accumulated abundant data which is invaluable for the design of ship models for sea testing, design and demonstration of testing schemes, installation and commissioning of equipment, and the construction of safeguarding systems for testing at sea. These experiments can be extended to various aspects of the ship and provide a good reference for other large-scale model tests. As an example, this study considers an energy-saving device (ESD) which includes a preswirl stator (PSS) and rudder bulb, and investigates the energy-saving function of the installed ESD (see Fig. 1).

2. Ship model setup

In this study, a glass fibre-reinforced plastic ship model is considered for sea testing. Modelled after the 230000DWT 'CSB FORTUNE' (a large-scale ore carrier) at a 1:13 scale, the model is a single-engine, single-propeller stern driven ship. With a block coefficient (C_B) of 0.83, the ship

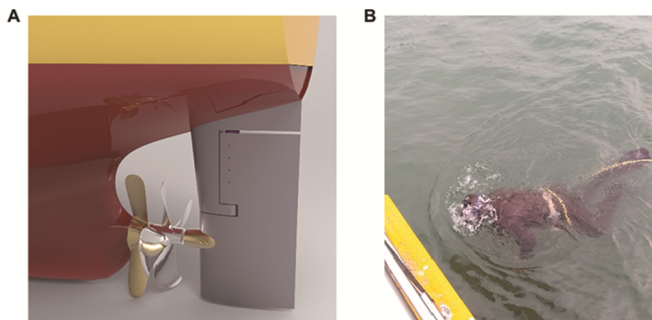


Fig. 1. Propeller and energy-saving device (ESD): (A) preswirl stator (PSS) and semi-spade rudder with rudder bulb installed at the stern of the ship model and (B) diver changing the ESD and propeller underwater.

model is that of a full form ship with a bulbous bow, parallel midbody, and transom stern. The main parameters are listed in Table 1.

Fig. 2 shows the layout of the ship model, which includes propulsion and autopilot systems (see Fig. 3) in the stern room, integrated navigation system and data collection system in the cab, and ballast blocks with a total weight of 95 tonnes.

The propulsion system comprises a console, 30 kW generator, integrated cabinet, servomotor, and reduction gear with a reduction ratio of 1/4, broken-shaft-type self-propulsion instrument, two couplings, and a shaft and propeller on the bottom platform of the stern room. Therefore, the rotating speed of the propeller can be controlled as required. The broken-shaft-type self-propulsion instrument (see Fig. 3C) can simultaneously measure the thrust and torque of the propeller of the 25-m-long ship model with high accuracy. Independently developed by us, it is the core technology of this propeller system. By dividing the units, it applies two independent structures to reanalyse the thrust and torque of the propeller; hence, the different strain units bear only the axial or circumferential deformation, avoiding crosstalk between the thrust and torque. The contactless torque sensor integrates the flexibility of digital signal conditioning with carrier amplifier technology, which significantly improves measurement accuracy.

The autopilot system is also driven by the generator and integrated cabinet. It comprises a servomotor and reduction gear with a reduction ratio of 1/10, transmission mechanism, rudder stopper, rudder stock, and semi-spade rudder body on the rear deck of the stern room. The integrated navigation system, which uses the global positioning system (GPS) and an inertial navigation system (INS), can monitor the 6-DOF motions of the ship model. The data collection system also contains two parts. The first part, embedded in the console, is used for collecting related information on the main engine, steering engine, and integrated navigation system, and for controlling the propulsion and autopilot systems in real time. The other part, connected to sensors, is used for recording data, such as the thrust and torque of the propeller and the accelerated speed of the fore, midship, and aft parts of the ship model. All sensors and the console are powered by batteries to separate the strong currents from the weak, thereby avoiding signal interference. As the deadweight of the ship model is relatively large, the selection and arrangement of the ballast blocks is considerably challenging. After careful design, concrete blocks and sandbags were used as ballast blocks and tiled on the hull bottom. Most of the ballast was loaded into the ship model while on the dock car; the remaining ballast was loaded into the ship model and levelled after launching.

3. Comprehensive test system

Fig. 4 shows a block diagram of the comprehensive test system for the resistance and propulsion performance of a ship model in actual seas. The comprehensive test system is divided into two parts, a resistance testing system and a self-propulsion testing system.

3.1. Resistance testing system

The first part of the comprehensive test system includes a system for resistance testing in a harbour. It is necessary to select a suitable harbour based on the testing needs. The factors to be considered include the length, water depth, experimental area infrastructure such as water, electricity, and winching equipment, and the wind and waves in the

Table 1
Main parameters of the ship model.

L_{oa}/m	L_{WL}/m	L_{PP}/m	B/m	D/m	d/m	∇/m^3	S/m^2	λ
24.99	24.62	24.20	4.04	1.87	1.39	115.2	144.75	1:13

L_{oa} – overall length; L_{WL} – length of water line; L_{PP} – length between perpendiculars; B – breadth; D – depth; d – draft; ∇ – displacement; S – wetted surface; λ – scale ratio.

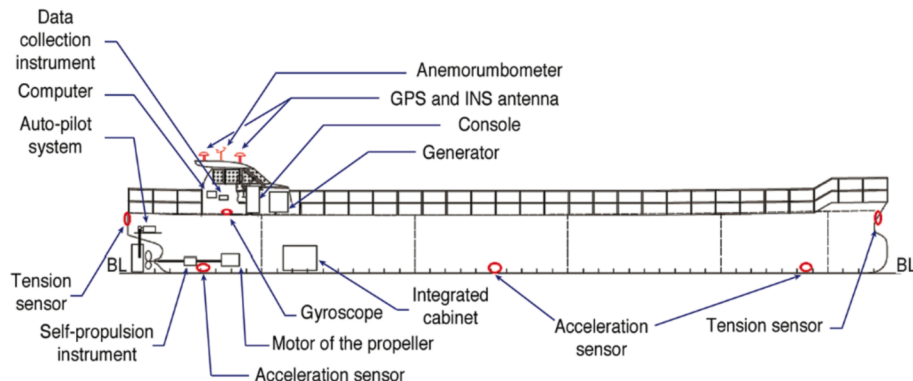


Fig. 2. Layout of the ship model.

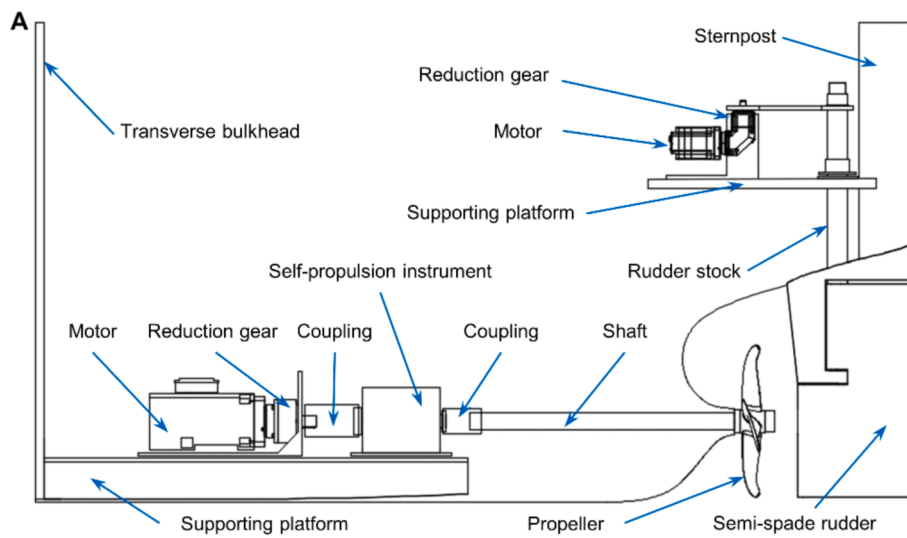
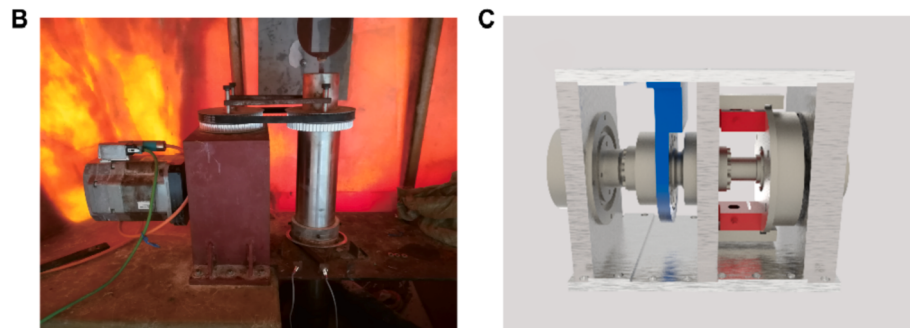


Fig. 3. Test equipment: (A) Layout of the propulsion system and autopilot system at the stern. The reduction gear of the propeller motor is connected to the broken-shaft-type self-propulsion instrument through a flexible pin coupling. The diameter of the stainless steel propeller shaft was set to 0.08 m, after considering the calculated value of the strength and the empirical value of the shipyard. (B) Transmission mechanism of the steering engine platform in the autopilot system, comprising a connecting rod and belt pulley. (C) Independently developed broken-shaft-type self-propulsion instrument connected to the propeller shaft through an expandable sleeve. High concentricity is required during installation.



harbour. After the arrangement of the ballast blocks, the ship model was launched by end launching. Its floating status was then adjusted to the designed waterline, and an auxiliary vessel was used to tow it to the experimental area.

Two high-power winches (see Figs. 5A and B, and 6) were installed diagonally in the harbour. Winch A, equipped with a frequency conversion control cabinet, permits manual input of the target rotating speed of the drum; it is used to haul the ship model such that it can sail at the required speed. Winch B, equipped with a brake apparatus, provides a pretightening force for the model; it is used to stabilise the sailing direction of the ship model and support the operation of winch A. On each side of the experimental area, a pulley was installed along the line connecting winches A and B to ensure that the ship model moves in the designated linear path during resistance testing. The error in the angle of

the force sensors relative to the line of the channel was less than 3°. The measurement error of the ship-model speed and resistance caused by the angle error was less than 0.4%, and could therefore be neglected. The two ends of the force sensors at the bow and stern of the ship were respectively connected to the hull and a rope through swivel hoist rings (see Fig. 7), preventing the ropes from breaking away from the sensors owing to circumferential forces.

The scheme for resistance testing is as follows: 1) A buoy-type wave weight instrument was launched before testing. Along with the anemorumbrometer (see Fig. 8), it measures and records the sea condition during the experiments, and ensures that the sea condition meets the requirements set in ISO 15016:2015 (the wind and wave levels should be below Level 2, and the wave height and wind speed must be less than 0.2 m and 3.4 m/s, respectively). Testing above the half-tide level (the

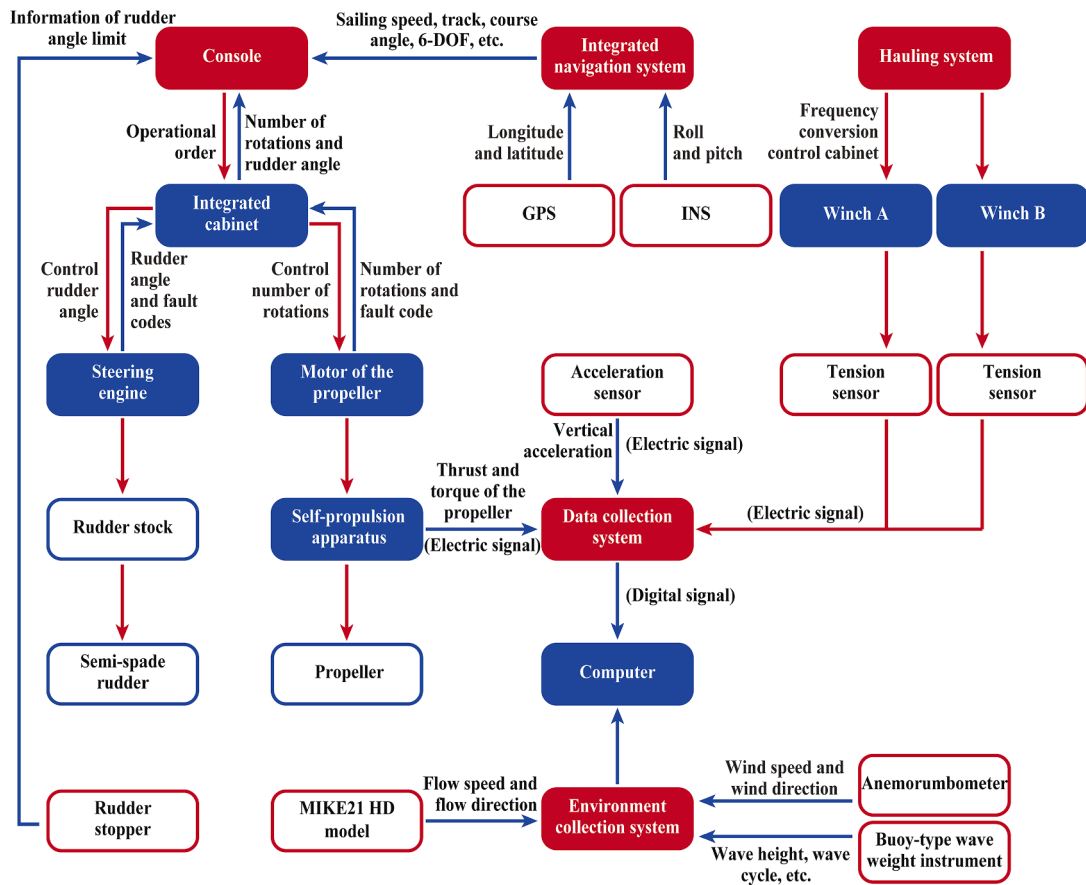


Fig. 4. Block diagram of the comprehensive test system for ship-model resistance and propulsion performance in actual seas.

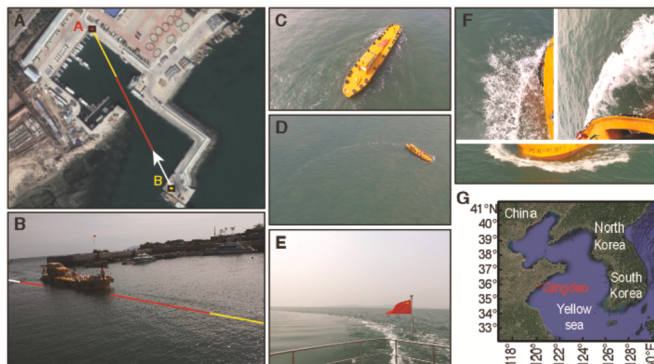


Fig. 5. Testing procedure of the 25-m-long ship model in actual seas: (A and B) Resistance testing in the harbour. The white line indicates the accelerating area, while the red and yellow lines indicate the measuring and decelerating areas, respectively. The length between the two winches was approximately 250 m, and the measuring area with effective data was approximately 100 m long. (C) Self-propulsion testing in actual sea waters; (D and E) wave formed at the stern when the ship model turns around; and (F) wave at the bow. (G) Location of the self-propulsion test at Qingdao in China.

corresponding depth of water was $d > 3\sqrt{BT}$ and the Froude depth number was $Fn_h < 0.5$) can eliminate shallow water effects (ITTC, 2017a). Moreover, the Froude depth number of the ship model does not vary along the track of the model in resistance testing. The width of the narrowest part of the channel was approximately twice the length of the ship model (see Fig. 5A). Further, the blockage (midship sectional area/channel cross section) was less than 2.0%. In this case, the sidewall effects are negligible, as stated in ITTC (2017a) and Xie et al. (1978).

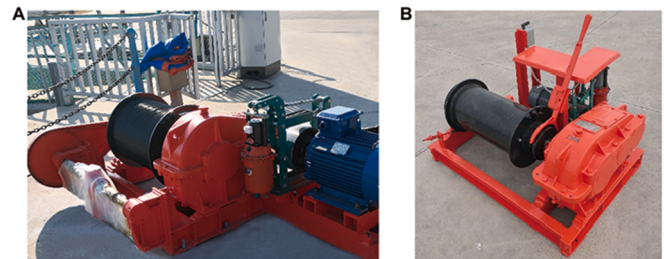


Fig. 6. Winches A and B: (A) Winch A (Motor power: 22 kW, rated pull: 6 kN, rated rotating speed: 0–3 m/s, drum diameter: 0.5 m, and rope capacity: 350 m); (B) Winch B (Motor power: 0.75 kW, rated pull: 1 kN, rated rotating speed: 0.4 m/s, drum diameter: 0.3 m, and rope capacity: 350 m). The winches were fixed to the ground through anchor bolts using light and high-strength Dyneema ropes (high-strength polyethylene fibre) with a diameter of 8 mm.

This was further confirmed by analysing the resistance data in the time domain, as no evident changes were observed when the ship passed through the boundary of the water area. 2) A security inspection was performed before testing to ensure normal equipment operation. 3) Winch A was used for hauling the ship model at a constant speed; it was maintained under horizontal tension and coincided with the centre line of the ship model during testing. 4) After the ship model entered the measuring area from the accelerating area and reached the speed required for testing, the force balance was used to obtain raw data for 40 s of measurement. The braking rope was then used to slow the ship model. 5) An auxiliary vessel was launched to assist the ship model in returning to the starting point, for testing under other working conditions. 6) The ESD (see Fig. 1B) was changed underwater to perform

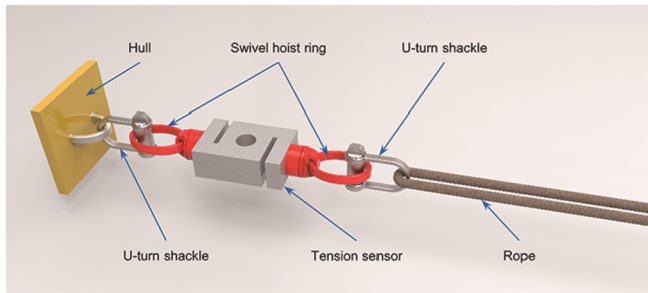


Fig. 7. Force sensors. The ends of the sensor are connected to the hull and rope through a swivel hoist ring and U-turn shackle, respectively. The range of the tension sensor is 1000 kg and the sensitivity coefficient is 0.5 mv/EU. One end of the rope is connected to the sensor at the bow and stern, while the other is connected to the winch. A thicker supportive braking rope is required for short-distance braking in the stern because of the relatively large inertia of the ship model; this allows the size of the testing area to be reduced and protects the sensor.

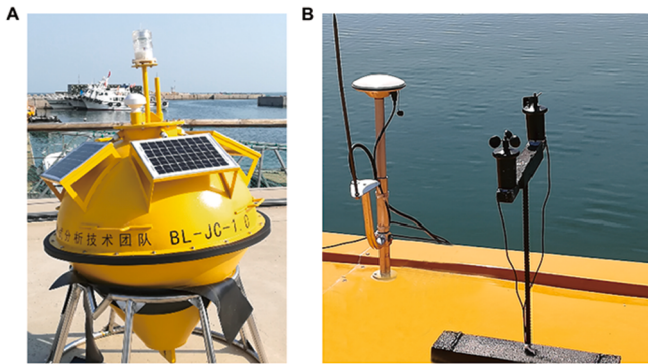


Fig. 8. Measuring and recording the sea condition: (A) Buoy-type wave weight instrument powered by solar energy (Wave height measurement range: 0–2 m, accuracy: $\pm 10\%$, distinguishability: 0.01 m); the measurement cycle ranges from 1.6 to 30 s, with an accuracy of ± 0.25 s. (B) Anemometer installed on top of the cab (Wind speed measurement range: 0.4–45 m/s, distinguishability: 0.1 m/s, accuracy: $\pm 2\% n + 0.1$ m/s, wind direction measurement range: 0–360°, and distinguishability: 22.5°).

fully appended resistance testing.

3.2. Self-propulsion testing system

The second part of the comprehensive test system includes a self-propulsion testing system used in actual seas. We accomplished self-propulsion testing in an actual sea, as depicted in Fig. 5C–5F. As shown in Fig. 5G, self-propulsion testing was conducted in sea waters 5 km from the shore of Qingdao. The water temperature of the testing area was approximately 21 °C, and the water depth was approximately 20 m.

Before testing, the weather forecast was checked to determine whether it was suitable for sea testing. Before starting the experiments, the ship model was towed to a suitable testing area by an auxiliary vessel. Initial testing was conducted with a ship speed of zero, which included the correction of the propeller torque and measurement of the wind speed and direction. During testing, an environmental collection system was applied for real-time monitoring of the wind, wave, and current flows, as shown in Fig. 4.

With reference to the testing method used in real ships, a scheme for the self-propulsion testing of ship models in actual seas was designed. During self-propulsion testing, a certain direction was considered as the reference. The ship model sailed in a straight line in a fixed direction at a constant propeller rotating speed. Data were collected once the sailing speed had stabilised. After at least 10 min of operation, testing was

conducted at different propeller rotating speeds, along with an increase in the number of rotations. When the ship model returned, the reference direction was rotated 180°, and the same testing procedure was performed. The speed of the ship model relative to the ground (V_G), and the thrust and torque of the propeller were measured during testing.

During the testing process, the auxiliary vessel was 500 m away in the convoy. A captain was on the ship model to mitigate potential dangers such as submerged reefs in the navigation area.

4. Data processing method

Combining the existing technologies and the achievements of tank model testing and full-scale ship testing in seas, we developed related technological methods suitable for ship-model testing in actual seas. For resistance testing in the harbour, the resistance value at a certain sailing speed can be obtained by calculating the difference between the two force balances at the bow and stern of the ship model. As actual sea conditions are complicated and continuously changing, to compare the various performance indicators of the ship model under different conditions during self-propulsion testing in actual seas, it is necessary to consider the methods proposed by Thomson (1978), ITTC (2017a), and ISO (2015). The testing data under actual sea conditions must then be revised, mainly considering the effects of tidal flows, wind resistance of the superstructure, and added resistance by the waves. The uncertainty of the test results was analysed according to the methods proposed by Aldous et.al. (2015), ISO (2008), and ITTC (2017b). The combined standard uncertainty ($u_c(y)$) was evaluated by the propagation of uncertainty, given by Eq. (1) (Park et al., 2015a; ITTC, 2008):

$$u_c(y) = \left[\sum_{i=1}^N \left(\frac{\partial f}{\partial x_i} \right)^2 u^2(x_i) + 2 \sum_{i=1}^{N-1} \sum_{j=i+1}^N \frac{\partial f}{\partial x_i} \frac{\partial f}{\partial x_j} u^2(x_i, x_j) \right]^{\frac{1}{2}} \quad (1)$$

where u is the standard uncertainty of the result of a measurement expressed as a standard deviation, $y = f(x_1, x_2, \dots, x_N)$ is the experimental result, and $\partial f / \partial x_i$ is the sensitivity coefficient of the sensor.

At low speeds, the ship model will be considerably affected by the water flow, causing it to yaw or even stop sailing. Therefore, the self-propulsion test was performed only when the ship's speed was greater than that of the current. It is necessary to select an appropriate revision method based on the tidal flows in the testing area. Given that every self-propulsion test duration of the ship model is considerably shorter than the tidal cycle, this study applied the mean of means (MoM) method to revise the sailing speed. For this revision, the ship model must operate six times at three different levels of horsepower of the main engine, with a steering angle below 5°, and the upper limit of the acceptable difference between the real and calculated values at 0.1 kN (Strasser et al., 2015). For accurate results, two round-trip runs under the same working conditions need to be conducted for testing, after which the MoM method can be applied to derive the following equation for revising the sailing speed.

$$V_m = \frac{V_{G1} + 3V_{G2} + 3V_{G3} + V_{G4}}{8} \quad (2)$$

The thrust and torque measurements of the propeller can also be revised using the MoM method. Self-propulsion testing is typically conducted in areas with a sufficient water depth. However, when it is necessary to adjust for the effects of shallow water and revise the speed ($\frac{A_M}{d^2} \geq 0.05$, where A_M is the underwater orthographic projection area and d is the water depth), the Lackenby method is suggested (Lackenby, 1963). Eq. (3) is used for calculating the incremental value of the revised speed (ΔV_G):

$$\Delta V_G = \left\{ 0.1242 \cdot \left(\frac{A_M}{d^2} - 0.05 \right) + 1 - \left[\tan d \left(\frac{gd}{V_G^2} \right) \right]^{\frac{1}{2}} \right\} \cdot V_G \quad (3)$$

As the windward area of the structure above the waterline (including the superstructure) is relatively large and the wind speed at sea is considerable, the air resistance cannot be ignored. The incremental value of the wind resistance (R_{AA}) can be calculated by Eq. (4), as proposed by ITTC (2018):

$$R_{AA} = 0.5\rho_A \cdot C_{DA}(\psi_{WRref}) \cdot A_{XV} \cdot V_{WRref}^2 - 0.5\rho_A \cdot C_{DA}(0) \cdot A_{XV} \cdot V_G^2 \quad (4)$$

where ρ_A is the density of air, A_{XV} is the area of the cross section that bears the maximum wind blow, V_{WRref} is the relative wind speed at the benchmark height, and ψ_{WRref} is the relative wind direction at the benchmark height ('0' indicates the windward direction, as shown in Fig. 9). The air drag coefficient, C_{DA} , can be obtained through a computational fluid dynamics (CFD) method, wind tunnel testing with relevant models or the relevant statistical information provided by ISO15016:2015 (ISO, 2015), or through the regression equation proposed by Fujiwara et al. (2005). The error in R_{AA} was less than 20%. The uncertainty introduced by R_{AA} , which mainly arises from the relative wind direction, was less than 25 N.

As self-propulsion testing of the ship model in actual seas cannot be conducted in still waters, the effect of waves on the sailing speed under actual sea conditions should be considered. When the heave and pitch of the ship model during testing are relatively small (the vertical acceleration of the bow is lower than 0.05 g), and the relative wave direction is below $\pm 45^\circ$, it is advisable to apply the STAwave-1 method (Boom et al., 2013). Eq. (5) is the empirical equation for the added resistance by the waves (R_{AW}), proposed by ITTC (2017a):

$$R_{AW} = \frac{1}{16}\rho_s g H_{W\frac{1}{3}}^2 B \sqrt{\frac{B}{L_{BWL}}} \quad (5)$$

where ρ_s is the density of water, g is the gravitational acceleration, $H_{W\frac{1}{3}}$ is the significant wave height of the wind waves, and L_{BWL} is the length of the bow on the water line at 95% of the maximum beam (see Fig. 9D). All self-propulsion tests were conducted at sea with $H_{W\frac{1}{3}} < 0.12$ m. The error in R_{AW} was less than 15% and the uncertainty introduced by R_{AW} was less than 10 N.

It is difficult to completely adjust the loading conditions of the ship model at sea to the standard loading conditions. However, this adjustment will cause the displacement of the ship model to differ from the standard displacement. Generally, a range of $\pm 2\%$ from the standard displacement is permitted for the actual displacement. Both ITTC

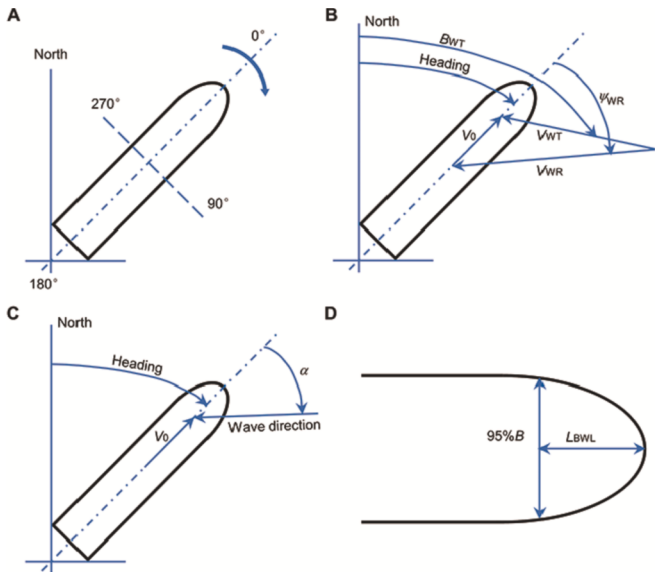


Fig. 9. Test scheme: (A) Sign conventions; Sign convention for (B) wind direction and (C) wave direction, and (D) Definition of L_{BWL} (ITTC, 2017a).

(2017a) and ISO (2015) apply Eq. (6) to calculate the incremental value of the resistance (R_{ADIS}) caused by the difference in displacement:

$$R_{ADIS} = 0.65R_m \left(\frac{\Delta_0}{\Delta} - 1 \right) \quad (6)$$

where Δ_0 is the standard displacement and R_m is the resistance of the ship model. The ship model, ballast, and equipment were weighed before loading. The error in Δ was less than 1%, and the relative uncertainty introduced by R_m was less than 5%.

Therefore, the resistance increment caused by wind, waves, and displacement deviations under actual sea conditions (ΔR) can be obtained using Eq. (7):

$$\Delta R = R_{AA} + R_{AW} + R_{ADIS} \quad (7)$$

Other factors such as yawing, steering, and changes in the water temperature and density of sea water only affect the sailing speed to a small degree and can therefore be ignored. Some of the results acquired through the above revision method are depicted in Fig. 10.

$$\eta_D = \frac{P_E}{P_{DB}} = \frac{R_x V / 75}{\eta_S \eta_G P_S} \quad (8)$$

where P_E is the effective power of the ship model, P_{DB} is the received power of propeller, η_S is the shafting transmission efficiency, η_G is the efficiency of reduction gear, and P_S is the power from the motor.

5. Results and discussion

Analysis of the resistance testing results revealed that the effect of the ESD on the incremental value of the resistance of the ship model increases with an increase in sailing speed (see Fig. 10A). R_x was the revised resistance based on the R_m obtained from the resistance testing and the resistance increment ΔR during self-propulsion testing (see Fig. 10B). The error in R_x was less than 8%.

The time series of the propeller thrust and torque with increasing propeller rotating speed in one test are presented in Fig. 11. Note that for each propeller rotating speed, both the propeller thrust and torque reach a steady state, which oscillates by about a mean value. In addition, the amplitudes of the torque are significantly larger than those of the propeller thrust.

There are evident scale effects in studies on the energy-saving function of ESDs (Shen et al., 2016). Therefore, it is meaningful to explore such functions of an ESD installed on the 25-m-long ship model. The performance of the propeller operating in natural seas (i.e. in actual seawater) differs from that in testing tanks, with lower Reynolds numbers. As shown by the results of the self-propulsion testing of the ship model in actual seas, the propulsive efficiency of the model improves significantly when the ESD is installed (see Fig. 10C). The propulsive efficiency appreciation of the ESD-installed propeller ($\Delta\eta_D$) increased with the ship's speed, reaching 2.92% at $Fn = 0.15$ during the self-propulsion testing.

Fig. 12 compares the results of the mooring test and the self-propulsion test; it indicates that when the advance speed of the propeller is zero, both the thrust and torque of the propeller are relatively high. The errors in the thrust and torque of the propeller measured by the broken-shaft-type self-propulsion instrument were less than 2% of the reading. When the ESD is installed, the thrust of the propeller increases, whereas its torque decreases; this verifies the energy-saving function of the ESD. The ESD achieves energy savings as follows: 1) the PSS produces favourable thrust by changing the direction of water flow (Park et al., 2015b); and 2) the rudder bulb prevents flow separation by weakening the hub vortices, improving the propulsive efficiency (Shin et al., 2012).

In a ship-model towing tank, the Kelvin wave of a ship model with a relatively wide breadth cannot unfold completely. Instead, it will reflect at the sidewalls of the tank. Combined with blockage effects, it is

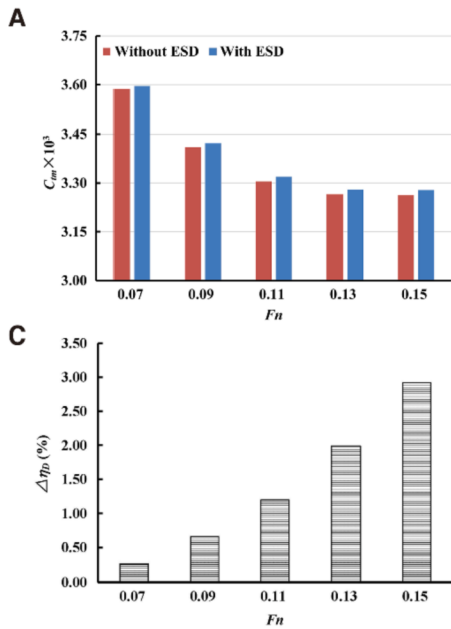


Fig. 10. Results of resistance and propulsion performance testing of the 25-m-long ship model in actual seas: (A) Curve of the variation pattern of the ship-model resistance coefficient (C_m) with respect to change in the Froude number (F_n) during resistance testing at harbour ($F_n = \frac{V}{\sqrt{gL_{WL}}}$); (B) Variation trend of the resistance after revision (R_x) with respect to change in F_n during self-propulsion testing in open water ($R_x = R_m + \Delta R$); (C) Variation pattern of the propulsive efficiency appreciation of the ESD-installed propeller ($\Delta\eta_p$) calculated using Eq. (8) with respect to change in F_n ; and (D) Image of the Kelvin wave captured by drones during self-propulsion testing of the 25-m-long ship model.

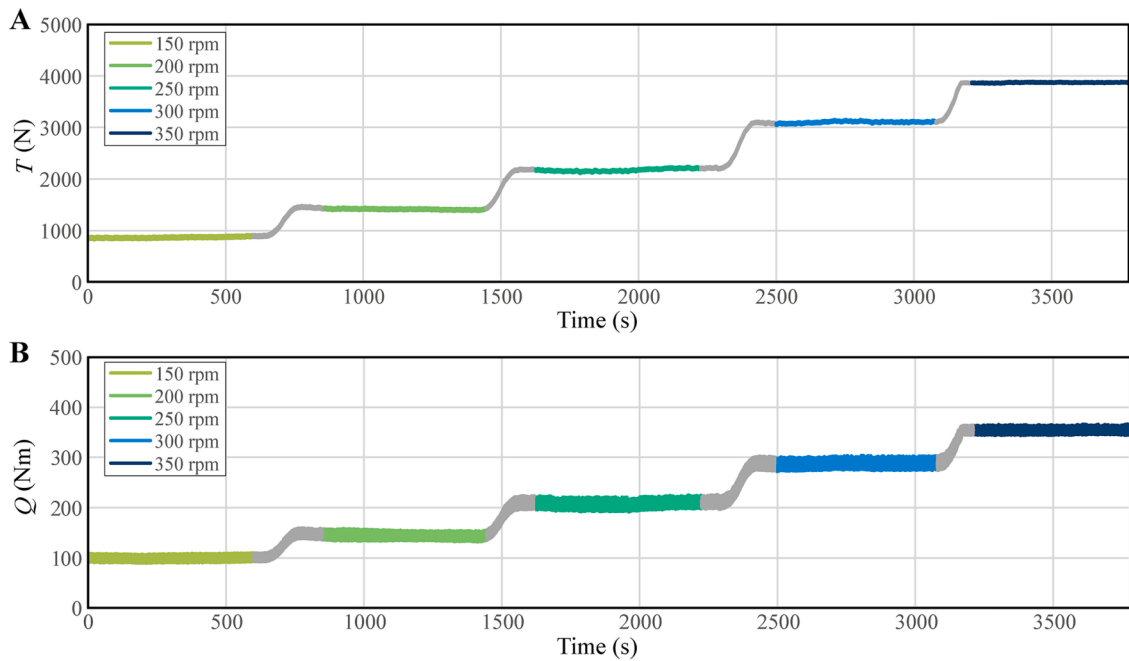


Fig. 11. Time histories of (A) propeller thrust T and (B) torque Q with increasing propeller rotating speed in one test.

impossible to obtain a perfect Kelvin wave. However, evident Kelvin waves can be obtained in the self-propulsion testing of a ship model in actual seas, as shown in Fig. 10D. The wakes of the ship model when it turns around are distinctive, as shown in Figs. 5D and E. The wave energy produced by the ship model during self-propulsion testing can be determined through the analysis of the waveform. Particle image velocimetry can be applied to monitor the characteristics of the flow field at typical positions of the ship model in actual seas to verify the CFD results.

6. Conclusions

In this paper, the scheme and results obtained for a comprehensive test system for ship-model resistance and propulsion performance in

actual seas were presented. The effects of an ESD on the ship performance under actual sea conditions were also assessed. The results established that the proposed technique is reliable, and the energy-saving function of the ESD was confirmed. The comprehensive test system and method can be used for diverse purposes, including as a reference guide for other large-scale model tests. The test system can be further improved by enhancing the test device accuracy and further optimising the data processing methods. With this system, conventional tests for the seakeeping performance and manoeuvrability can be extended. In addition, related equipment can be installed to perform specific tests, such as ship underwater explosion tests and tests for the exciting force of the propeller. It is expected that more ship models will be constructed by applying this comprehensive test system to a ship model in actual seas to enhance test data and verify and optimise the

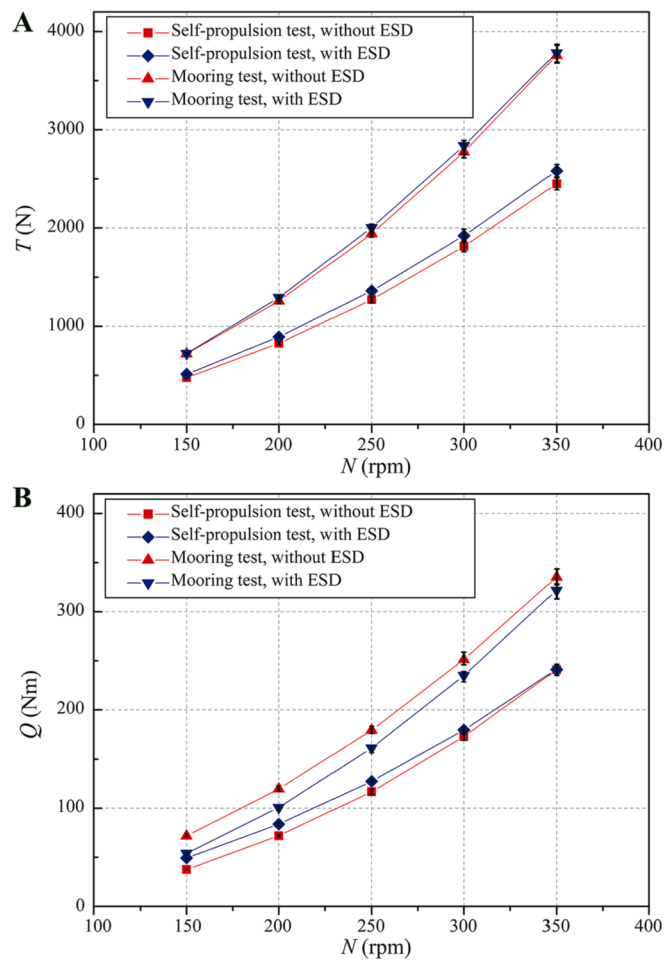


Fig. 12. Variation patterns with error bars of (A) propeller thrust T and (B) propeller torque Q with respect to changes in rotating speed.

testing schemes and test result handling methods, which can pave the way for remarkable achievements in the near future.

Author contributions section

Jian-feng Lin: Investigation, Formal analysis, Writing- Original draft preparation. **Da-gang Zhao:** Methodology, Investigation, Writing - Review & Editing. **Chun-yu Guo:** Conceptualization, Resources, Project administration. **Yu-min Su:** Supervision, Validation. **Xiang-hai Zhong:** Data curation, Investigation.

Funding

This work was supported by the National Natural Science Foundation of China [grant number 51709060], the Fundamental Research Funds for the Central Universities [grant number HEUCFM180104] and the Foundation of Key Laboratory of Defense Science and Technology for Equipment Pre-research (China) [grant number 61422230203182223010].

Declaration of competing interest

The authors declare that they have no known competing financial interests or personal relationships that could have appeared to influence the work reported in this paper.

Acknowledgement

This work was in response to the research project titled, ‘High Technology Ship Scientific Research Project’ by the Ministry of Industry and Information Technology [MIIT2016, 548] (China).

References

- Aldous, L., Smith, T., Bucknall, R., Thompson, P., 2015. Uncertainty analysis in ship performance monitoring. *Ocean Eng.* 110, 29–38. <https://doi.org/10.1016/j.oceaneng.2015.05.043>.
- Andersen, I.M.V., Jensen, J.J., 2014. Measurements in a container ship of wave-induced hull girder stresses in excess of design values. *Mar. Struct.* 37, 54–85. <https://doi.org/10.1016/j.marstruc.2014.02.006>.
- Boom, H., Huisman, H., Mennen, F., 2013. New Guidelines for Speed/Power Trials: Level Playing Field Established for IMO EEDI. SWZ Maritime, Schip en Werf de Zee Foundation Rotterdam.
- Bouscasse, B., Broglia, R., Stern, F., 2013. Experimental investigation of a fast catamaran in head waves. *Ocean Eng.* 72 (7), 318–330. <https://doi.org/10.1016/j.oceaneng.2013.07.012>.
- Coraddu, A., 2013. Analysis of twin screw ship’s asymmetric propeller behaviour by means of free running model tests. *Ocean Eng.* 68, 47–64. <https://doi.org/10.1016/j.oceaneng.2013.04.013>.
- Fossati, F.V., Bayati, I., Orlandini, F., Muggiasca, S., Vandone, A., Mainetti, G., Sala, R., Bertorello, C., Begovic, E., 2015. A novel full-scale laboratory for yacht engineering research. *Ocean Eng.* 104, 219–237. <https://doi.org/10.1016/j.oceaneng.2015.05.005>.
- Fujiiwara, T., Ueno, M., Ikeda, Y., 2005. A new estimation method of wind forces and moments acting on ships on the basis of physical component models. *JASNAOE* 2, 243–255. <https://doi.org/10.2534/jjasnaoe.2.243>.
- Gong, J., Guo, C.Y., Song, K.W., Wu, T.C., 2019. SPIV measurements and URANS simulations on the inlet velocity distribution for a waterjet-propelled ship with stabiliser fins. *Ocean Eng.* 171, 120–130. <https://doi.org/10.1016/j.oceaneng.2018.11.002>.
- Grigoropoulos, G.J., Katsaounis, G.M., 2004. Measuring procedures for seakeeping tests of large-scale ship models at sea. In: Proceedings of the 13th IMEKO TC4 Symposium on Measurements for Research and Industrial Applications, pp. 135–139.
- ISO, 2008. Uncertainty of Measurement – Part 3: Guide to Expression of Uncertainty in Measurement (GUM: 1995). ISO/IEC Guide 98-3” (Geneva Switzerland).
- ISO, 2015. Ships and Marine Technology – Guidelines for the Assessment of Speed and Power Performance by Analysis of Speed Trial Data. ISO 15016” (British Standards).
- ITTC-Recommended Procedures and Guidelines, 2008. 7.5-02-01-01 (Revision 01), Guide to the Expression of Uncertainty in Experimental Hydrodynamics, 25th ITTC.
- ITTC-Recommended Procedures and Guidelines, 2017. 7.5-04-01-01.1 (Revision 07), Preparation, Conduct and Analysis of Speed/Power Trials, 28th ITTC.
- ITTC-Recommended Procedures and Guidelines, 2017. 7.5-02-03-01.2 (Revision 01), Uncertainty Analysis, Example for Propulsion Test, 28th ITTC.
- ITTC-Recommended Procedures and Guidelines, 2018. 7.5-02-07-02.8, Calculation of the Weather Factor F_w for Decrease of Ship Speed in Wind and Waves, 29th ITTC.
- Jiao, J.L., Sun, S.Z., Li, J.D., Adenya, C.A., Ren, H.L., Chen, C.H., Wang, D.J., 2018. A comprehensive study on the seakeeping performance of high speed hybrid ships by 2.5D theoretical calculation and different scaled model experiments. *Ocean Eng.* 160, 197–223. <https://doi.org/10.1016/j.oceaneng.2018.04.051>.
- Lackenby, H., 1963. The effect of shallow water on ship speed. *Shipbuilder Machine Eng.* 70, 446–450. <https://doi.org/10.1111/j.1559-3584.1964.tb04413.x>.
- Loukakis, T., Grigoropoulos, G., Katsaounis, G., Corrigan, P., 2005. Large Scale Model Testing at Sea (Seakeeping Committee of ITTC, 3).
- Nielsen, D.M., Stredulinsky, D.C., 2012. Sea state estimation from an advancing ship—A comparative study using sea trial data. *Appl. Ocean Res.* 34, 33–44. <https://doi.org/10.1016/j.apor.2011.11.001>.
- Noblesse, F., Huang, F., Yang, C., 2013. The Neumann–Michell theory of ship waves. *J. Eng. Math.* 79 (1), 51–71. <https://doi.org/10.1007/s10665-012-9568-7>.
- Park, D.M., Lee, J., Kim, Y., 2015a. Uncertainty analysis for added resistance experiment of VLCC2 ship. *Ocean Eng.* 95, 143–156. <https://doi.org/10.1016/j.oceaneng.2014.12.007>.
- Park, S., Oh, G., Rhee, S.H., Koo, B.Y., Lee, H., 2015b. Full-scale wake prediction of an energy saving device by using computational fluid dynamics. *Ocean Eng.* 101, 254–263. <https://doi.org/10.1016/j.oceaneng.2015.04.005>.
- Quintana, V., 2007. User-centered design in a large-scale naval ship design program: usability testing of complex military systems-DDG 1000. *Nav. Eng. J.* 1, 25–33. <https://doi.org/10.1111/j.0028-1425.2007.00001.x>.
- Ribeiro, S., Guedes, C., 2013. Prediction of parametric rolling in waves with a time domain non-linear strip theory model. *Ocean Eng.* 72, 453–469. <https://doi.org/10.1016/j.oceaneng.2013.07.011>.
- Shen, H.L., Omweri, O.E., Su, Y.M., 2016. Scale effects for rudder bulb and rudder thrust fin on propulsive efficiency based on computational fluid dynamics. *Ocean Eng.* 117, 199–209. <https://doi.org/10.1016/j.oceaneng.2016.03.046>.
- Shin, K.W., Lundgren, E., Nielsen, J.R., 2012. CFD-based Optimization of Rudder Bulb System. WMTC2012, St. Petersburg, Russia.
- Strasser, G., Takagi, K., Werner, S., Hollenbach, U., Tanaka, T., Yamamoto, K., Hirota, K., 2015. A verification of the ITTC/ISO speed/power trials analysis. *J. Mar. Sci. Technol.* 20 (1), 2–13. <https://doi.org/10.1007/s00773-015-0304-7>.
- Sun, S.Z., Ren, H.L., Zhao, X.D., 2015. Experimental study of two large-scale models’ seakeeping performance in coastal waves. *Brodogradnja* 66 (2), 47–60.

- Thomson, G.R., 1978. BSRA Standard Method of Speed Trial Analysis. NS 466[R]. BSRA Report.
- Wang, L.Z., Guo, C.Y., Xu, P., Su, Y.M., 2018. Analysis of the performance of an oscillating propeller in cavitating flow. *Ocean Eng.* 164, 23–39. <https://doi.org/10.1016/j.oceaneng.2018.06.036>.
- Xie, K.Z., Zhou, Z.Q., Song, J.J., Shen, H.Y., Ye, B.J., 1978. Experimental study on the blocking effect of pools. *Ship Res.* 02, 1–27.
- Zhao, D.G., Guo, C.Y., Su, Y.M., Wang, L.Z., Wang, C., 2017. Numerical study on the unsteady hydrodynamic performance of a four-propeller propulsion system undergoing oscillatory motions. *J. Coast. Res.* 33 (2), 347–358. <https://doi.org/10.2112/JCOASTRES-D-16-00007.1>.